17

STEWARD-1532

FERMILAB
SEP 3 1999
LIBRARY

PREPRINTS of the STEWARD OBSERVATORY

THE UNIVERSITY OF ARIZONA
TUCSON, ARIZONA 85721-0065 U.S.A.

No. 1532

Fermilab Library
0 1160 0071064 9

MILLIMETER AND SUB-MILLIMETER ASTRONOMY

T.L. WILSON
Sub-Millimeter Telescope Observatory, Steward Observatory
The University of Arizona, Tucson, AZ
and
Max-Planck-Institut f. Radioastronomie, Bonn, Germany

NAME | I D No. | M.S.
FERMILAB LIBRARY

SUBMITTED TO THE ENCYCLOPEDIA OF ASTRONOMY & ASTROPHYSICS
ED. BY P. MURDIN

Millimeter and Sub-Millimeter Astronomy

T. L. Wilson
Sub-Millimeter Telescope Observatory, Steward Observatory, The University of Arizona
Tucson, Az.
and
Max-Planck-Institut f. Radioastronomie, Bonn, Germany

1 Introduction

The millimeter wavelength band extends from λ=4 mm (ν=75 GHz) to 1 mm (300 GHz) while the sub-millimeter band extends from 1 mm to 100 μmeters (3 TeraHz). The sub-mm band is rather unexplored because of the need to construct large efficient telescopes and sensitive detectors. It is equally important to select excellent sites to reduce the pervasive absorption by the earth's atmosphere. To a lesser degree, these challenges also affect mm astronomy. Usually the emission from astronomical objects in the mm and sub-mm wavelength range is small compared to that in the meter and centimeter wavelength ranges where intense non-thermal synchrotron emission is common, or in the mid- and near-infrared or optical wavelength ranges, where thermal radiation from hot sources is found. Studies in the mm and sub-mm ranges cover a wide range of topics: (1) The physics and chemistry of the interstellar medium (ISM), especially the structure and content of molecular clouds, (2) Star formation, (3) The interaction of stars with molecular clouds, especially during the very early and very late phases of stellar evolution, (4) The distribution of molecular clouds (and neutral carbon) in external galaxies and high-redshift objects, and (5) Studies of solar system objects. Investigations of the 2.73 K background are also important but specialized.

Spectral line radiation from molecular hydrogen is rare since H_2 has no permanent dipole moment. Thus, extraordinary excitation conditions are needed. The properties of molecular clouds are traced using abundant polar molecules such as carbon monoxide, CO. In the mm and sub-mm wavelength ranges, small linear molecules have rotational transitions, while atomic and

ionized carbon have fine structure lines. In addition to gas, clouds contain dust grains which contain much of the silicon and carbon. Dust grain emit broadband thermal emission which increases at shorter wavelengths where these grains radiate more efficiently. The surfaces of cold grains are covered with condensed atoms and molecules.

There is a sudden transition from neutral atomic hydrogen, HI to H_2 from competition between destruction by the interstellar radiation field and production on grain surfaces. The envelopes of molecular clouds consist of neutral hydrogen, H I, and ionized or neutral carbon, with molecules in cloud cores.

1.1 A Short History

Observations started with broadband continuum measurements of emission from the Sun, planets and a few Quasi-Stellar Objects. Molecular spectroscopy provided a great impetus for mm and sub-mm astronomy. Radio spectroscopy of molecules began with the detection of the OH radical at a wavelength of λ=18cm in 1963. These molecules were thought to exist in HI regions. In 1968 the detection of the ammonia, NH_3, and water vapor, both at 1.3cm, was made with the Berkeley 6-meter telescope. In 1969, formaldehyde, H_2CO, was discovered with the National Radio Astronomy Observatory's (NRAO) 140-foot telescope at 6cm. The structures of H_2CO and NH_3 are rather complex, and the abundances are rather small. The most widespread polar molecule, CO, was detected at 2.6 mm in 1970 with the NRAO 36-foot telescope. After the discovery of CO, there was a rapid increase in the number of interstellar molecules, because radiation processes are more efficient at shorter wavelengths, and because there are a larger number of spectral lines in the millimeter and sub-millimeter wavelength ranges. As of 1999, 120 molecules have been found in the ISM; the heaviest molecule is $HC_{11}N$.

2 Technical Considerations

From diffraction theory, the angular resolution, θ, is

$$\theta = 1.2\lambda/\mathrm{D}$$

Where D is the telescope size and λ the wavelength. For a 10-meter diameter telescope, at λ = 3mm, θ = 80″. Intensities are expressed in terms of temperatures, in the Rayleigh-Jeans limit:

$$\mathrm{T} = \frac{\lambda^2 I_\nu}{2k} \tag{1}$$

Where k is Boltzmann's constant. I_ν is the intensity at frequency ν in units of Watts Hz^{-1} m^{-2} $\mathrm{steradian}^{-1}$. T is the "brightness temperature". For thermal emission from planets, T is the surface temperature diluted by the ratio of source to beam size broadened by the source. In most cases, T is not related to a physical source temperature. In terms of I, the Flux Density is

$$\mathrm{S}_\nu = \int I_\nu \mathrm{d}\Omega \tag{2}$$

The solid-angle integration is usually over the beam; if the source size exceeds the telescope beamsize, the integration is over the source. Combining Eq. 1 and 2, we have

$$\mathrm{S}_\nu = \frac{2k}{\mathrm{c}^2}\,\mathrm{T}\nu^2\,\Delta\Omega \tag{3}$$

The power received is

$$\mathrm{P}_\nu = \frac{1}{2}\mathrm{S}_\nu\,\mathrm{A}_{\mathrm{eff}}\,\mathrm{B} \tag{4}$$

Where $\mathrm{A}_{\mathrm{eff}}$ is the effective area and B is the bandwidth.

2.1 Receivers

For λ >0.3mm, the most efficient receivers for spectral lines are heterodyne systems. In such *coherent* receivers, the signal is converted from the sky wavelength to a longer wavelength at which the signal is amplified. Such systems have a wavelength resolution, $\lambda/\Delta\lambda \gg 10^6$. In the 1960's, receiver noise temperatures, T_{rx}, were ~5000K at 3mm; now, typical values are <100K. The ultimate limit for noise in a coherent receiver is $h\nu/\mathrm{k}$; practical limits are a few times larger. The first conversion is usually performed in a mixer. The first mixers were uncooled Schottky devices. Since the 1980's, mixers have junctions which are quantum mechanical Superconducting-Insulating-Superconducting (SIS) sandwichs. SIS mixers are much more sensitive and

require less local oscillator power than classical Schottky devices; SIS mixers must be cooled to 4 Kelvin. All such receivers are tunable over a large wavelength range. The development of SIS receivers in the millimeter and sub-mm range has been led by the Caltech Sub-mm Observatory (CSO) and in the millimeter range by NRAO. Other active SIS development groups are at Harvard-Smithsonian Center for Astrophysics (CfA), IRAM and Köln University. From the physics of junction materials, there is a short wavelength limit to the operation of SIS devices. For spectral line measurements at wavelengths, at λ <0.3mm, a new device, the Hot Electron Bolometer (HEB), which has no such limit, has been developed. The first successful astronomical measurements with HEB's were carried out by the CfA group on the Heinrich Hertz 10-m Sub-mm Telescope (HHT) in 1998. At λ >3mm, High Electron Mobility Transitors (HEMT's) are becoming standard, while at $\lambda > 2.6$mm, monolithic indium phosphide microwave transistor amplifiers (MIMIC's) are now being used on the 16-beam receiver array (SEQUOIA) installed on the University of Massachusetts 14-m telescope. Only SEQUOIA and the 8-beam SIS array installed on the NRAO 12-m telescope have thus far produced published results; all other millimeter heterodyne systems with competitive noise temperatures are single-beam devices.

Bolometers are *incoherent* receivers; these are preferred for single-dish measurements of broadband continuum radiation at λ <2 mm. As with heterodyne receivers, the sensitivity of Bolometers has improved greatly since the 1960's. Bolometer sensitivity is given as Noise Equivalent Power (NEP) in Watts $\mathrm{Hz}^{-1/2}$. For practical Bolometer systems, background noise, including noise from warm telescope surfaces, the ground and atmosphere is the limiting factor. A good value of NEP is 3 10^{-17} W $\mathrm{Hz}^{-1/2}$. For λ <0.3 mm, a combination of Bolometer detectors and Fabry-Perot filters can be effectively used for spectroscopy. In contrast to heterodyne systems, a number of bolometer array receivers are installed on telescopes. The largest is SCUBA, an 81-beam system on the James Clerk Maxwell 15-m Telescope (JCMT) in Hawaii.

The RMS receiver noise in Kelvin is

$$\Delta \mathrm{T}_{\mathrm{rms}} = \frac{\mathrm{A} \cdot \mathrm{T}_{\mathrm{sys}}}{\sqrt{\mathrm{B}\,t}} = \frac{\mathrm{A} \cdot \mathrm{NEP}}{2\,k\,\mathrm{B}\sqrt{t}} \tag{5}$$

The constant A is a function of system and data-taking parameters; usually A$\sim$2; B is the bandwidth in Hz and t is integration time in sec. The value

of B is limited to one-third of the linewidth for spectral line measurements. For continuum measurements, B can be much larger. The value used for T_{sys} is corrected for absorption of the signal in the earth's atmosphere and the emission from the earth's atmosphere and telescope losses. Depending on weather, the value of T_{sys} can exceed T_{rx} by large factors.

2.2 Telescopes

For a radio telescope to be effective, the surface accuracy must be < 0.1 of the shortest wavelength measured. Larger radio telescopes have surfaces consisting of individual panels which must be adjusted. The limit to the effective operation of all single telescopes is set by surface deformations and pointing errors. Some of the mm telescopes, with diameters of 14-meters and one with 20-meters, were built in radomes. The two largest millimeter telescopes, the 30-meter, operated by IRAM, and the 45-meter in Nobeyama, Japan, are in the open, as will be the 50-meter "Large Millimeter Telescope" (LMT) being constructed near Mexico City. The LMT is designed to be the most advanced single dish design, useful up to 345 GHz. The construction of open air telescopes is in part economic; enclosures could cost as much as the telescope itself. The most important improvement in the design of large single dishes has been *homology* a scheme in which a paraboloid freely deforms but the shape is maintained. The remaining systematic effects are the influence of wind and temperature gradients in the structure which give rise to differential thermal expansion in the structure. The first radio large telescopes built with high accuracy surfaces of low-expansion material, Carbon-Fiber-Reinforced-Plastic (CFRP), were the IRAM 15-meter interferometer antennas on Plateau de Bure, France and the 15-m Swedish-ESO-Sub-mm-Telescope (SEST) telescope, at La Silla, Chile and the 10-meter Heinrich-Hertz sub-mm telescope. The surface accuracy of the HHT shows that RMS surface accuracies of 12μmeters are possible. The 10.4-meter diameter telescope of the Caltech Sub-mm Observatory (CSO), and the 15-m JCMT are sub-mm telescopes on Mauma Kea, Hawaii, an excellent site. The CSO and JCMT were put into operation in the late 1980's and have produced a great deal of science. Both are constructed of aluminum and are housed in astronomical dome-like shelters.

Sub-mm measurements are also made from aircraft. The Kuiper Airborne Observatory provided such an opportunity with a 91-cm diameter paraboloid.

The follow-up facility, SOFIA, will have a 2.5-m diameter mirror. At normal flight altitude, 14 km, the water vapor content is extremely low. Thus, SOFIA can be used for measurements at wavelengths at which the atmosphere is opaque from ground-based sites. SWAS, the Sub-mm Wavelength Astronomy Satellite, has detected emission from the ground-state transition of H_2O, at 0.55 mm, but has not detected emission from O_2. In the future are the Far-Infra-Red-Satellite-Telescope, FIRST, and Satellite-Infra-Red-Telescope-Facility, SIRTF.

Single telescopes have a fixed relation of A_{eff} and θ whereas Interferometer systems do not (see Eq. 1 to 4). Present interferometer systems consist of $n < 11$ elements, each of a moderate diameter. Interferometers consist of a number of parabolic antennas, each equipped with one or more coherent receivers. The receiver outputs are combined to produce a response corresponding to the maximum angular resolution determined by the ratio of the wavelength to the largest separation of the elements, projected in the source direction. Emission from structures with angular sizes larger than the angle corresponding to the closest separation of the antennas are not recorded. This is the 'smooth structure' in a source. Such information can be recovered by combining the interferometer output with data taken using a large single telescope. Interferometers provide higher angular resolutions and positional accuracies than single dish telescopes. For a fixed collecting area bandwidth, and ν, the *temperature* (but not the Flux Density) uncertainty of an interferometer is worse than that for a single telescope with the same angular resolution. The first mm-wave interferometer, at the Berkeley Radio Astronomy Laboratory, consisted of two 6-meters antennas. In the mm range, there are 4 systems: The Berkeley-Illinois-Maryland association (BIMA) array near Hat Creek, Ca., the Caltech Owens Valley Interferometer (OVRO) near Bishop, Ca., the Nobeyama Array in Japan and the IRAM array on Plateau de Bure, France. A number of high dynamic range, high sensitivity images have been produced by the BIMA, OVRO and IRAM arrays. In addition, the 10-meter CSO and 15-meter JCMT telescopes are occasionally used as a sub-mm interferometer. To obtain even higher angular resolutions, experiments have been carried out using the technique of Very Long Baseline Interferometry (VLBI) at 3mm and 1.3mm. Finally, a dedicated Sub-mm Array consisting of eight 6-m dishes has been under construction by the Smithsonian Astrophysical Observatory and the Academica Sinica Institute for Astronomy and Astrophysics, Taiwan, on Mauna Kea,

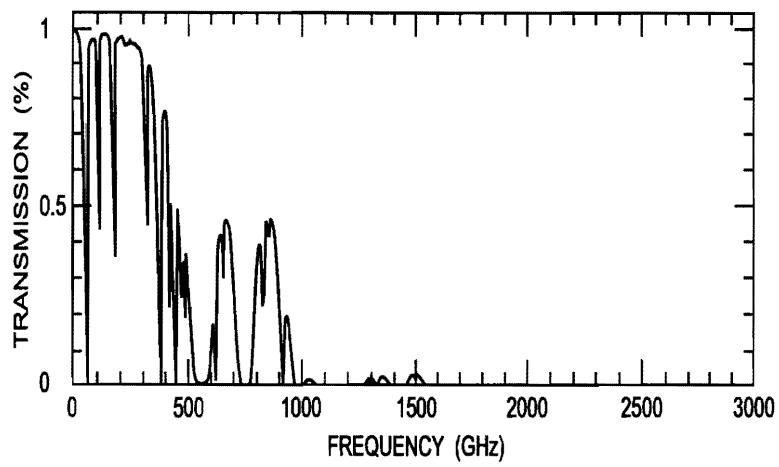

Figure 1: A plot of the transmission through the earth's atmosphere for the mm and sub-mm wavelength ranges, for a column density of atmospheric water vapor of 1mm. For an atmospheric optical depth τ, the transmission is $e^{-\tau}$. (adapted from Phillips & Keene 1992).

Hawaii. The sensitivity and imaging quality of interferometer systems can be improved by an array with many large antennas on an excellent site. This is the rationale of the ALMA ('Atacama Large Millimeter Array') project, to be built in Chile at 5 km elevation, by NRAO and ESO. ALMA is planned to have $n > 60$ elements and a total $A_{eff} > 10^4 m^2$. The results to be obtained with ALMA may revolutionize all of astronomy.

2.3 Atmospheric Effects

Millimeter and especially sub-mm observing sites are selected to minimize the effect of weather on the observations. Signals are absorbed by O_2 and H_2O Vapor. The scale height of H_2O vapor is ~2 km, while that of O_2 is ~8 km, so the influence of H_2O should be reduced at high altitudes. See Fig. 1 for a plot of transmissions. At 860 GHz (λ=0.35 mm), even the very best sites on earth are useful only a small percentage of the time.

2.4 Observing Techniques

Because the signal levels are small compared to atmospheric or receiver noise, all measurements must be made by taking the difference of two signals. For spectral line measurements, one uses compares data taken at two different positions or frequencies; for continuum measurements there is a rapid switching by movements of the telescope subreflector or by wobbling a flat mirror. The time intervals are determined by instabilities in the receiver and atmosphere. A technique of slow scanning of the telescope is the normal data taking mode for continuum measurements. For spectral line measurements this has been called "on-the-fly" mapping. The data are taken rapidly, before weather or telescope characteristics can change. This greatly increases the reliability of spectral line images and efficiency of data taking.

"Chopper wheel" calibrations are the norm for spectral line measurements. In the simplest version of this method, measuremenents are made of a room temperature absorber and the atmosphere; with models, these allow an estimate of the atmospheric emission and hence the absorption. A more complete characterization of the atmosphere requires a "tipping curve", which involves measurements at a number of elevations. The data are corrected for the absorption and usually for telescope efficiencies to give intensities (usually in the form of temperatures) for a perfect telescope outside the atmosphere. Additional calibration steps involve measurements of sources of known intensity, then scaling the data taken. For interferometry, the measurements of a source and known source or "calibrator" are interspersed in time. It is assumed that the system performance varies smoothly between calibrations, and the corrections obtained are applied to the source measurements.

3 Astronomical Considerations

3.1 Spectral Lines

In Fig. 2 we show the energy level diagrams for CO, neutral carbon, C I, and ionized carbon, C II; the energy, E, above the ground state in Kelvins, from E=kT. Allowed dipole transitions occur with a unit change in the angular momentum quantum number $\Delta J = \pm 1$. For the CO molecule low-J transitions are frequently thermalized, so the kinetic temperature, T_k, characterizes the populations. Measurements of CO allow good estimates of the

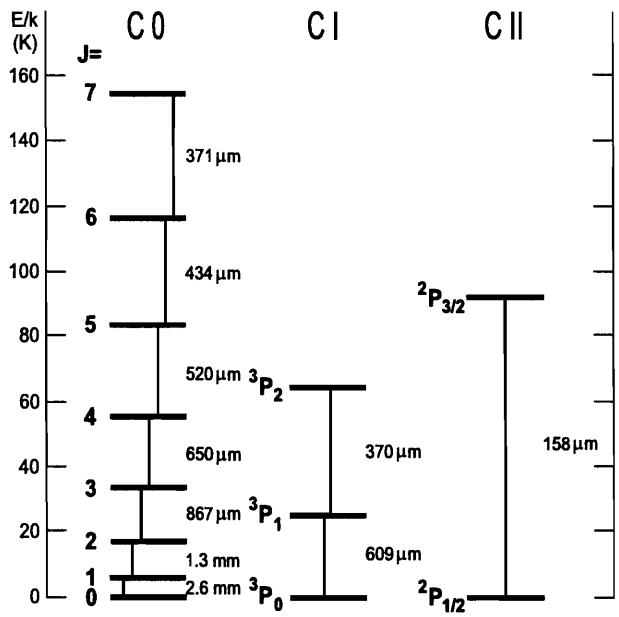

Figure 2: The first few rotational energy levels of selected species. In the ISM, carbon monoxide, CO, is the most abundant molecule with a permanent dipole moment. Also shown are fine structure transitions of neutral carbon, C I, and ionized carbon, C II.

column density of H_2, since CO can be excited at low H_2 densities, since the excitation close to Local Thermodynamic Equilibrium (LTE), and since there is a large abundance relative to H_2.

If the radiation arises from an isothermal layer much larger than the telescope beam, one can obtain a fairly realistic estimate of kinetic temperatures and CO column densities using an LTE analysis. Rotational lines of $^{12}C\,^{16}O$ are usually optically thick, then peak line temperature T equals T_k, the kinetic temperature. To obtain column densities without models of molecular clouds, one must use rarer, stable isotopes of CO. In LTE, the total population, N can be obtained from the (optically thin) $J = 1 - 0$ line of $^{13}C^{16}O$:

$$N(\text{total})^{13}_{\text{CO}} = 2.6 \cdot 10^{14} \frac{T \int \tau^{13}(v)\mathrm{d}v}{1 - \exp\{-5.3/T\}} \,. \tag{6}$$

where the column density $N(\text{total})^{13}_{\text{CO}}$ is in cm^{-2}, the linewidth v in km s^{-1}, and T in Kelvins. If the line optical depth, $\tau^{13} \ll 1$, $T\tau^{13}=T^{13}_{L}$. If $\tau^{13} \gg 1$, we must use the line of $C^{18}O$; the expression is very nearly the same. Such estimates are usually realistic for cooler clouds (T_k <20K). To obtain the column density of H_2, one assumes an isotopic ratio, and that the CO to H_2 ratio is 10^{-4}; the latter value is usually reasonable.

In addition to estimates of column densities, one can estimate local H_2 densities, $n(H_2)$ from the ratio of column density to cloud size to obtain the local density. This leads to a lower limit for $n(H_2)$ since clouds have small scale structure or "clumping". If energy levels are populated by collisions with H_2 molecules, the density needed to balance decay out of a level is n^*. Setting the collision rate equal to the decay rate, we have $n^* \sigma \bar{v}=A$. If the optical depth of the line is $\tau \gg 1$, the analysis becomes more complex. In the Sobolev or Large Velocity Gradient (LVG) approximation, one assumes that the molecular cloud has a velocity gradient $V \sim r$. In the LVG model, the value of the A coefficient is replaced by A/τ. For a multi-line analysis of a species, including the fall-off above and below the maximum intensity, one can solve for both T_k and H_2 density (see Fig. 3).

From LVG calculations applied to optically thin transitions of carbon monoxide, there is a simple relation between total column density and the $J = 2 - 1$ line, which is valid for a wide range of kinetic temperatures and H_2 densities. Large scale surveys of ^{13}CO and CO $J = 1 \rightarrow 0$ lines in the disk of our Galaxy show that line shapes and intensity ratios along lines-of-sight are remarkably similar. Since ^{13}CO lines are optically thin, the CO

integrated line intensities must measure mass, even though $\tau^{12} \gg 1$. This can be explained if clouds are in Virial equilibrium, and consist of a large number of small sub-thermally excited clumps. An exact relation between integrated intensity of the $J = 1 \rightarrow 0$ line and column density of H_2 has been determined empirically for the disk. This approach has been often used for molecular mass determinations in external galaxies. However, there are exceptions to this relation: The conversion factor for the galactic center is 1/7 of the factor used for the disk, and the conversion factor appears to differ from galaxy to galaxy.

3.2 Dust Emission

Another method to determine H_2 column densities is to use broadband dust emission. The dust intensities rise rapidly with frequency, and measurements made with large bandwidths lead to very small values of ΔT_{RMS} (see Eq. 5). One drawback to continuum measurements is line-of-sight confusion, since there is no velocity information. The quantitative relation between τ_{dust} and $N(H_2)$ is calibrated by the measurement of emission and extinction toward NGC 7023. The optical extinction has been converted into a column density of hydrogen using the standard gas-to-dust relation (see Mathis 1990 Ann. Reviews A & A 28, 41). If $h\nu \ll kT$:

$$N(\mathrm{H}) = 1.93 \cdot 10^{15} \frac{S_\nu}{\theta^2} \frac{\lambda^4}{Z/Z_\odot \, b \, T_{dust}} \, . \tag{7}$$

S_ν is in Jy, source FWHP size, θ, in arc seconds, and λ in μm. $N(\mathrm{H})$ is the column density of hydrogen in all forms, in cm^{-2}. The value of metallicity is Z (for the Sun, $Z_\odot$). The factor b accounts for changes in grain sizes. For moderate densities, $b = 1.9$; for very dense gas, $b = 3.4$, but a wider range is likely. If the uncertainties in Eq. 7 can be reduced, dust measurements could rival molecular line determinations of mass estimates. Images of dust emission show more structure than images of spectral lines; the explanation for this is not clear, thus far.

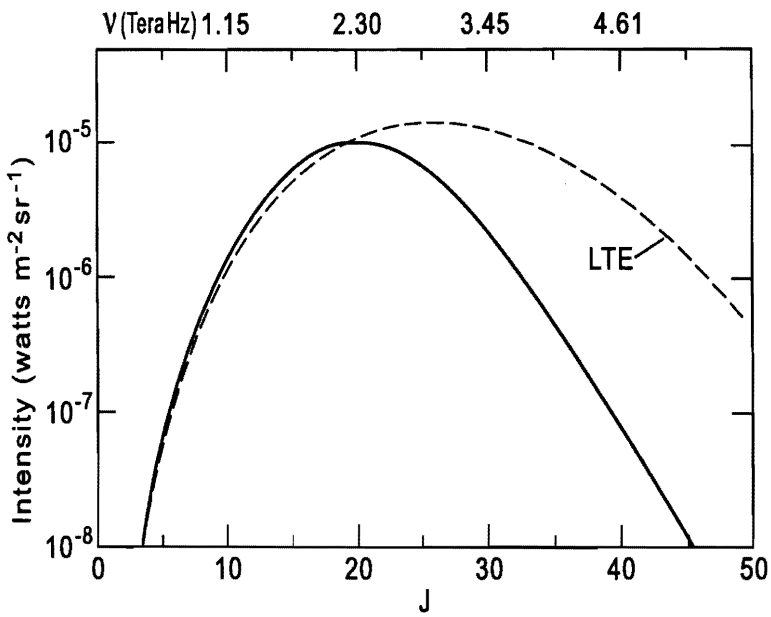

Figure 3: A plot of CO line intensities for the Orion KL source. The dashed line is a plot of populations for LTE, while the solid line is an LVG calculation for T_k=750K, $N(H_2)$=2.8 10^{21}cm^{-2}, $n(H_2)$=2.7 10^6cm^{-3}. The difference in the curves is caused by the faster decays from higher J levels. With measurements at frequencies above and below than the maximum, one can determine both $n(H_2)$ and T_k (Watson et al. 1985 ApJ 298, 316).

4 A Summary of Scientific Results

It is estimated that there are ~5000 **Giant Molecular Clouds** in our galaxy. These each have masses of $\sim 10^6$ $M_\odot$; these are probably cloud complexes with, on average, $n(H_2) \approx 10^2 cm^{-3}$and $T_k \approx 20K$. Dark Dust Cloud have larger densities and T_k=10K. Clouds are assumed to be gravitationally stable, and may have a fractal structure. For the galactic disk inside the Solar circle, the mass in HI and H_2 are about equal. Outside the solar circle, the mass of HI is ~6 times that of H_2.

In most clouds, $\Delta v_{1/2}$, the FWHP linewidths, are found to be supersonic. There are some exceptions, such as the denser cores of dark clouds. Large–scale organized motions, such as rotation, or large scale collapse are ruled out from observations. It is unlikely that magnetohydrodynamic waves cause most of the line broadening. The linewidths could be caused by outflows from embedded objects, such as young stars or by the conversion of large scale motions such as galactic rotation into smaller-scale turbulence. These motions cause **shock waves** which give rise to broader lines. Theoretical studies show that there are two types of shocks: 'J' or jump shocks and 'C' or continuous shocks. J-shocks locally heat the gas and this leads to the dissociation of molecules. This will change the chemistry of the cloud greatly. C-shocks are cushioned by larger magnetic fields and cause less dissociation. Sub-mm line ratios provide a diagnostic which allows one to differentiate between these types of shocks. For J-shocks, there is a large amount of emission from ions. For C-shocks, the emission is primarily molecular and neutral carbon, but little ionic emission. For a complete understanding, studies of CO, C I and C II are needed (energy level diagrams in Fig. 2).

The most well-studied galactic sources are (1): IRC+10216, a circumstellar envelope of the Red Giant star CW Leo. This source is ~150pc from the Sun, (2) The Orion KL region, at 500pc. This source is 45″NW of the Trapezium cluster of stars which ionize the Orion H II region, with FWHP 10″, T_{kin}=165K, and $n(H_2)=10^7 cm^{-3}$, (3) The dark cloud center TMC-1 in Taurus, with T_{kin}=10K, and $n(H_2) \sim 10^4 cm^{-3}$ at 160 pc, (4) SgrB2, a complex of dense H_2 clouds and HII regions at 8.2 kpc, near the center of our Galaxy, and (5) Sgr A, the galactic center itself. In addition, there are a number of well studied external galaxies. The group is inhomogeneous for a number of observational reasons; the objects are Arp 220, IC342, M82, M51 and NGC 253. In the mm range, all of these were first mapped to a resolu-

tion of $\sim 12''$ in a number of lines with single dishes. Later the brighter lines were imaged with interferometers down to resolutions of $\sim 2''$. References to data are given at the end of this section. See especially references in the *Protostars and Planets* series.

Interstellar **chemistry** involves non–equilibrium, non–terrestrial processes. At typical densities, neutral-neutral gas phase reactions are too slow to form complex molecules in $\sim 10^6$ years. Rather, the formation involves ion-molecule chemistry. Hydrogen and helium ions are produced by cosmic rays. The H^+ forms H_3^+, or charge exchanges with C or O atoms. The reaction rates for ion–molecule reactions are $>10^3$ times faster than neutral reactions. This explains the abundance of molecules such as CO or OH in dark clouds. Ion-molecule reactions also play a large role in the formation of molecules in the envelopes of low mass stars in the Red Giant phase. As a rule–of–thumb, hydrogen–poor molecules with unsaturated bonds are gas–phase, ion-molecule products, while molecules with saturated bonds are thought to be produced on grains and released into the ISM.

An important goal of mm and sub-mm astronomy is to determine **collapse criteria** for molecular clouds, and to search for individual collapse objects. Stars must form from molecular clouds, because of the close spatial and physical associations. Models for collapse begin with sizes of 10^{16}cm, continuing to pre-planetary disk sizes 10^{14} cm around the resulting star. At present, mm and sub-mm instrumentation limits us to nearby objects which could be imaged on scales $<10^{16}$ cm. After many searches, a number of candidate objects have been found. These are mostly in Dark Dust Clouds where low mass stars are expected to form. The collapse signature is based on a model where the cloud center has higher temperature and density, and where the collapse motions exceed the thermal motions. The measurements of optically thick lines, such as carbon monosulfide, $^{12}C^{32}S$ will show a narrow absorption feature (from gas in the outer part of region). This locates the center of the emission profile. If the cloud is collapsing, the blue shifted portion of this profile has a larger intensity than the red-shifted portion, since the radiation from hotter blue-shifted gas passes through the red-shifted gas without being absorbed. The red-shifted radiation from equally hot gas is absorbed by cooler gas at nearly the same velocity. Thus the blue wing arises closer to the warmer gas. If the cloud is expanding, the red-shifted portion is more intense. A measurement of the rarer isotope $^{13}C^{32}S$ must show no narrow absorption feature or asymmetry.

An important aspect of molecular cloud physics involves **cooling**. There are theoretical models, but these are complex even in idealized cases. Surveys of mm and sub-mm spectral line data allow direct tests of the cooling processes by mapping the intensities of the lines of CO, which dominates cooling at lower densities and H_2O, which should dominate at higher densities. At the highest densities, one expects that hydrides will provide most of the cooling. Measurements of the CO lines from J=1 to 20, H_2O transitions and lines from the more abundant hydrides are needed to experimentally determine the heat flow from clouds.

Fundamental to the star-formation process is the **outflow** phase. This occurs shortly after the core of the star forms. Excess material is expelled in the form of a bipolar high velocity stream of material which is mainly molecular. Such outflowing material has been traced in mm wavelength lines of CO and other molecules. The central object in this phase is a Young Stellar Object, or YSO. Surrounding the YSO is usually a dense disk of material, perpendicular to the direction of the bipolar outflow; outflows may be driven by magnetic forces.

A completely different type of outflow occurs at the end of the Main Sequence life of stars of roughly a few solar masses. These Asymptotic Giant Branch (AGB) stars or Red Giants, are referred to as mass loss stars. Many have been traced in CO lines. The outflow velocities are $\sim$30 km s^{-1}. The mass loss mechanism is thought to be radiation pressure on dust grains, which drags the gas. The moderate velocity flows are sometimes accompanied by flows with velocities larger than 100 km s^{-1}. This material should be hotter and may be atomic rather than molecular. If so, atomic lines of carbon or oxygen might supplement the information based on CO or shock tracers such as SiO, to trace these flows.

In **Photodissociation Regions**, the molecules are close to a source of Ultraviolet radiation which alters the chemistry and heat balance. The most obvious change is that CII and CI become much more abundant. The layer containing CI may extend to a depth which is a significant fraction of the width of the PDR. The most well known PDR is the 'Orion Bar', to the SE of the Orion H II region.

Sub-mm spectroscopy of **Galaxies** is likely to reveal warmer regions of exceptional star-forming or shock activity. Since most galaxies are compact, high angular resolution is needed. Some have moderately intense lines, so can be imaged with interferometers. For most, the emission is usually weak,

so lower resolution data is taken with single telescopes, so far. The most studied galaxy in the mm and sub-mm is Messier 82. It has long since been established that M 82 has warm molecular gas; there are HHT maps over a few arc minutes in the J=7–6 line of CO which arises from an energy level 156K above ground. Thus, there must be very widespread emission from warm molecular gas; details of the heating processes are not fully understood. Another interesting object is the galaxy Centaurus A. The nucleus is an intense continuum emitter even in the sub-mm wavelength range, so that species such as hydrides might be detected in absorption. Another fruitful case study is the face-on spiral IC342, thought to be an analog of our Milky Way. Studies will allow a comparison of global properties of these sources. At red shifts >4, CO lines have been detected in the mm wavelength range. In the future, the detection of redshifted lines of molecules, CII and OI would extend chemistry studies to the early universe. See the results summarized by Combes & Wiklind in *Highly redshifted Radio Lines* 1998, Astronom. Soc. of the Pacific Conference Series 156, ed. C.L. Carilli et al.

Further Reading

A good reference for sub-mm studies is R. Genzel, 1991 in *Galactic Interstellar Medium*, ed. W. B. Burton et al. For the fundamentals of radio astronomy and mm line studies of molecular clouds, see Rohlfs & Wilson 1996 *Tools of Radio Astronomy.* Both are published by Springer-Verlag, Heidelberg. A recent review of mm and sub-mm interferometric results and techniques is by A. I. Sargent & W. J. Welch 1993 Ann. Rev. Astron. Astrophys. 31, 297. Sub-mm work is reviewed by T. G. Phillips & J. Keene 1992 Proc. IEEE 80, 1662. Scientific results are summarized in *Protostars and Planets III*, 1993, ed. E. H. Levy & J. I. Lunine, Univ. of Arizona Press, and *The Molecular Astrophysics of Stars and Galaxies*, 1998, ed. T. W. Hartquist & D. A. Williams, Oxford Univ. Press.